spectral range as predicted by theory. Regenerative amplifiers having variable pulse widths have been implemented in OMEGA and GDL. All measurements agree well with the calculations made from that simple theory. This analysis lends itself to many other systems such as systems with resonant reflectors, multimirror cavities, etc. It can also be used for an injected pulse having an arbitrary temporal profile or phase modulation.

ACKNOWLEDGMENT

This work was supported by the U.S. Department of Energy Office of Inertial Confinement Fusion under Cooperative Agreement No. DE-FC03-92SF19460, the University of Rochester, and the New York State Energy Research and Development Authority. The support of DOE does not constitute an endorsement by DOE of the views expressed in this article.

REFERENCES

1. LLE Review **50**, 71 (1992).
2. M. D. Skeldon and S. T. Bui, to be published in the *Journal of the Optical Society of America B*.
3. M. D. Skeldon, S. T. Bui, S. Letzring, and W. Siryk, in *Solid State Lasers III*, edited by G. J. Quarles (SPIE, Bellingham, WA, 1992), Vol. 1627.
4. M. Born and E. Wolf, *Principles of Optics*, 5th ed. (Pergamon Press, Oxford, 1975).
5. J. D. Gaskill, *Linear Systems, Fourier Transforms, and Optics* (Wiley, New York, 1978).
6. A. Papoulis, *Systems and Transforms with Applications in Optics* (McGraw-Hill, New York, 1968), p. 379.
7. W. Koechner, *Solid-State Laser Engineering* (Springer-Verlag, New York, 1988), p. 218; "Fused silica," Technical Rep. (Corning, Inc., MP-21-4, Corning, NY, 14831).

1.F Shaping of Nanosecond Linearly Chirped Pulses

The importance of detailed laser pulse shapes in optical communications, ultrafast spectroscopy, and laser fusion has seen increasing recognition recently. Pulse shaping has traditionally been difficult to perform, and no approach has been entirely successful in achieving the goals of fast rise time, flexibility, stability, and contrast. Laser pulses have been shaped by performing techniques in time domain, frequency domain, or in a combination thereof.[1] Time-domain

pulse-shaping techniques, which include gain saturation (or saturable absorption), acousto-optic, and electro-optic techniques, have been proposed for certain temporal modulations. Frequency-domain pulse shaping,[2–11] which is accomplished by using diffraction gratings, has the capability of producing a wide range of picosecond and femtosecond pulse shapes and has been used in both optical communications and ultrafast spectroscopy.

In laser inertial-confinement fusion, relatively long pulses with detailed pulse shapes are required to influence the fusion capsule's implosion dynamics.[12] Useful pulse-shaping techniques should be able to provide both nanosecond pulses and flexible pulse shapes. Time-domain, electro-optical pulse-shaping techniques, which have long been studied, have difficulty achieving 100-ps response times and accurately controlled flexible pulse shapes. Frequency-domain pulse-shaping techniques (well known for their flexibility) therefore become the candidates for laser-fusion technological research.

Frequency-domain pulse shaping, however, is usually applied to ultrashort pulses where their relatively broad bandwidths allow for easy separation of the frequency components of the laser beam within a reasonable distance (~1 m).[5–11] In laser fusion, because of other requirements such as beam smoothing[13] and frequency conversion,[14] the laser bandwidth must often be carefully limited. The difficulty of stretching and shaping a narrow-band, ~60-ps laser pulse from a mode-locked oscillator to ~10 ns has limited the application of spectral pulse-shaping techniques in laser fusion.[4] Skupsky *et al.* recently proposed a spectral-beam-deflection, pulse-shaping scheme using an electro-optical device to encode the laser beam with phase-modulated bandwidth for spectral pulse shaping.[1] The advantage of this scheme is that after pulse shaping the laser beam can be sent into an inverse electro-optical device to remove the encoded phase modulation and narrow the bandwidth. This scheme would reduce the bandwidth concern of using spectral pulse shaping in laser fusion. However, appropriate electro-optical devices are not yet available for use in this application.

This article reports on the stretching and shaping of nanosecond linearly chirped pulses using an all-optical, passive, two-grating pulse-shaping system.[2–7] We focus on the temporal response of a linearly chirped pulse shaped by a unit-step spectral mask (a sharp edge at the spectral plane). The rise time is studied as a function of the laser bandwidth, frequency chirp, and the spectral resolution of the pulse-shaping system. We have also designed a lens system placed inside the two-grating pulse-shaping system to provide the large effective grating separation and control the spectral resolution for the shaping and stretching of narrow-band pulses. Laser pulses are originally generated from an Nd:YLF mode-locked oscillator. A single-mode optical fiber is used to produce the required bandwidth. These pulses are then sent to the passive two-grating system for stretching and shaping. The benefit of the passive pulse-shaping system is its simplicity, flexibility, and reproducibility. The bandwidth concern, associated with very fast rise-time applications, can be solved by using Skupsky's scheme[1] once the active electro-optical device is available for bandwidth generation and reduction.

Basic Equations

The fundamental frequency-domain pulse-shaping scheme was invented by E. B. Treacy in 1969.[2] Two parallel gratings were originally used for pulse compression or expansion. This scheme was later extended for pulse shaping by introducing a spectral mask and a retro-reflecting mirror after the grating pair.[3] Figure 53.31 shows a similar scheme with the use of transmission gratings operating in the Littrow configuration. The spectral angular dispersion Γ ($\equiv d\theta/d\lambda$) is generated when the laser beam passes through the first grating.

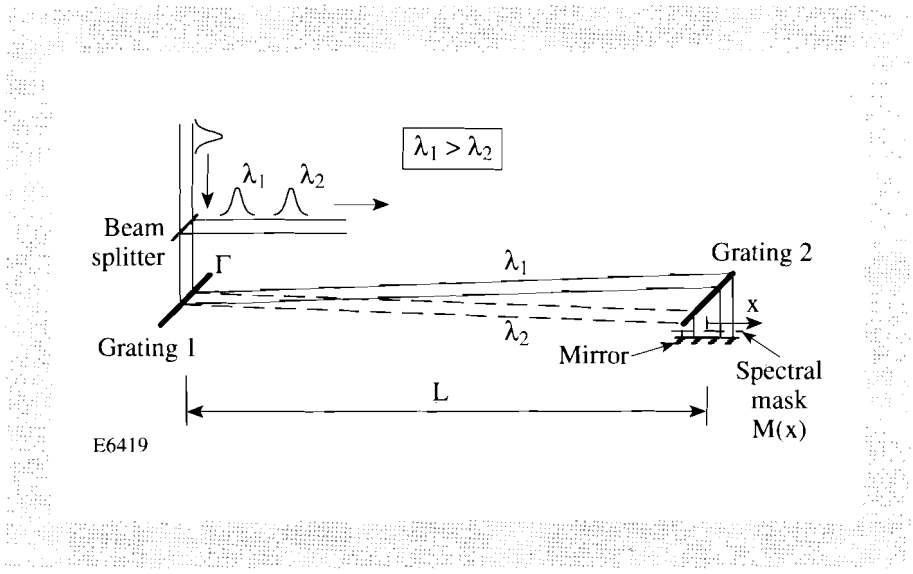

Fig. 53.31
The basic pulse-shaping and stretching scheme. Two representative waves λ_1 and λ_2 show the spectral dispersion and group delay.

After the dispersive laser beam propagates a distance L, its spectral angular dispersion is cancelled by the second grating, which has the same groove spacing as the first grating but an opposite incidence angle. The grating pair spatially separates the frequency components of the input laser pulse. The phase and/or amplitude of these spectral components are then modified by a spectral mask. Upon returning through the grating pair, these modified spectral components are recombined to form the desired pulse shape. Two representative waves λ_1 and λ_2 depict the spatial separation and group delay between different frequency components. Note that the distance traveled by the λ_1 component is longer than the distance traveled by the λ_2 component. This produces a linearly chirped pulse. Because of the linear relationship between frequency and time, a linearly chirped pulse can be shaped in the frequency domain and then mapped directly into the time domain.

The function of the two-grating pulse-shaping system shown in Fig. 53.31 can be expressed by one stretching function and one spectral-filtering function. The stretching function can be expressed as $\exp(ik_0L\beta^2\omega^2)$ in the frequency domain,[2] where ω is the frequency shift from the central frequency ω_0, k_0 is the wave vector at central frequency ω_0, L is the grating separation, and

$\beta \equiv d\theta/d\omega = -(\lambda^2/2\pi c)\Gamma$ describes the angular dispersion. The spectral-filter function for this system, with a Gaussian beam of waist w_o located at the spectral mask $M(x)$, is[7]

$$S(\omega) \equiv \sqrt{\frac{2}{\pi w_o^2}} \int_{-\infty}^{\infty} M(x) \exp\left[-2\left(x - \frac{dx}{d\omega}\omega\right)^2 / w_o^2\right] dx \,. \tag{1}$$

For the particular pulse-shaping scheme shown in Fig. 53.31, $dx/d\omega = \beta L$. If we consider only the frequency-dependent terms, we can write the stretched and shaped pulse as

$$E_{out}(\omega) = E_{in}(\omega) \exp\left(ik_o L\beta^2\omega^2\right) S(\omega) \,, \tag{2}$$

where $E_{in}(\omega)$ and $E_{out}(\omega)$ represent the input and output pulses in the frequency domain, respectively. Equations (1) and (2) are well studied in pulse compression and spectral pulse shaping. In this article we apply these two equations specifically to pulses with a large frequency chirp.

Spectral pulse shaping can be represented more intuitively by using the following three parameters: the length spanned by all frequency components on the spectral mask Δx; the group delay $\Delta\tau$ between the limiting spectral components; and the spectral resolution N. For a laser pulse with a bandwidth $\Delta\omega = -(2\pi c/\lambda^2)\Delta\lambda$ passed through the grating pair as shown in Fig. 53.31, the spatial separation of the frequency components can be understood by the simple geometric relation

$$\Delta x = \beta L \Delta\omega = \Gamma L \Delta\lambda \,. \tag{3}$$

This equation simply depicts the space-frequency relation $dx/d\omega = \beta L$ for Eq. (1). The group delay introduced by the system (round trip) is $4\Delta x \tan\theta/c$, where θ is the grating angle in the Littrow mode. By using Eq. (3) and $\beta \equiv d\theta/d\omega = 2\tan\theta/(k_o c)$, this group delay can be rewritten as $2k_o\beta^2 L\Delta\omega$. For an input chirped pulse $E_{in}(\omega) = A_{in}(\omega)\exp[i\phi_{in}(\omega)]$, where $A_{in}(\omega)$ and $\phi_{in}(\omega)$ are real functions, the total phase shift of the output shaped pulse shown in Eq. (2) is equal to

$$\phi(\omega) \equiv \phi_{in}(\omega) + k_o\beta^2 L\omega^2 \,,$$

and the total group delay of the output shaped pulse becomes[2]

$$\Delta\tau = \frac{d^2\phi(\omega)}{d\omega^2}\Delta\omega = \left[\frac{d^2\phi_{in}(\omega)}{d\omega^2} + 2k_o\beta^2 L\right]\Delta\omega \,. \tag{4}$$

The spectral resolution N is related to the the parameter Δx and is defined as[7]

$$N \equiv \Delta x / w_o \,, \tag{5}$$

where w_o is the Gaussian beam waist at the spectral mask. It is important to note that as the beam waist w_o approaches zero the spectral resolution approaches infinity, and the spectral filter function $S(\omega)$ approaches exactly the same shape as the spectral mask $M(x)$.

Unit-Step Spectral Filtering

To understand the space-frequency-time relationship in spectral pulse shaping, we focus on the case of a pulse with a large frequency chirp shaped by a sharp edge placed at the spectral plane; that is, shaped by a unit-step spectral mask

$$M(x) = \begin{cases} 0 & x < x_1 \\ 1 & x \geq x_1 \end{cases} . \tag{6}$$

The spectral filter function described by Eq. (1) can be solved as[7]

$$S(\omega) = \frac{1}{2}\left\{1 + erf\left[\sqrt{2}\left(\omega - \frac{\Delta\omega}{\Delta x} x_1\right) \Big/ \left(\frac{\Delta\omega}{N}\right)\right]\right\} , \tag{7}$$

where $\Delta\omega$ is the input laser bandwidth, N is the spectral resolution, and $\Delta\omega/\Delta x = 1/(\beta L)$ for the scheme shown in Fig. 53.31. The spectral filter function described by Eq. (7) is a smooth curve related to the error function. For an input pulse with a uniform spectrum across the sharp edge, the function $|S(\omega)|^2$ describes the shaped power spectrum near the sharp edge. The rising edge of the power spectrum spans a spectral width $\Delta\omega/N$. For the same spectral mask and the same input pulse, the shaped pulse described by Eq. (2) can be solved as

$$E_{out}(t) = \frac{1}{2}\exp\left[i\left(\omega_o t - \frac{2t^2}{\tau_{min}^2}\right)\right]\left\{1 + erf\left[e^{-i\frac{\alpha}{2}}\sqrt{2}\left(t - \frac{\Delta\tau}{\Delta x} x_1\right) \Big/ \tau_r\right]\right\} , \tag{8}$$

where *erf* is the complex error function and ω_o is the central frequency of the input laser. The time-space relation $\Delta\tau/\Delta x = [d^2\phi(\omega)/d\omega^2]/(dx/d\omega)$ can be obtained by combining Eqs. (3) and (4). The phase α is defined as

$$\alpha \equiv \tan^{-1}\left[\frac{4}{w_o^2}\left(\frac{dx}{d\omega}\right)^2 \Big/ \frac{d^2\phi(\omega)}{d\omega^2}\right] = \tan^{-1}\left(\frac{4N^2}{\Delta\omega\Delta\tau}\right) , \quad 0 \leq \alpha \leq \frac{\pi}{2} . \tag{9}$$

Later we will show that the parameter α is an indication of the intensity (energy) rippling of the shaped pulse. For an input transform-limited pulse, that is,

$\phi_{in}(\omega)=0$, the phase α can be simplified as $\alpha=\tan^{-1}(L/z_R)$, where L is the grating separation and $z_R=k_0 w_0^2/2$ is the Rayleigh range of the Gaussian beam. The two time constants τ_{min} and τ_r in Eq. (8) are defined as

$$\tau_{min} \equiv 2\sqrt{\frac{d^2\phi(\omega)}{d\omega^2}} = 2\sqrt{\frac{\Delta\tau}{\Delta\omega}}\ , \tag{10}$$

$$\tau_r \equiv \frac{\tau_{min}}{\sqrt{\sin\alpha}}\ . \tag{11}$$

The time constant τ_r can be treated approximately as the rise time of the shaped pulse, which is defined as the time required for the laser intensity to rise from 10% to 90% of its final value. (When α is small, the time constant τ_r is equal to 0.95 rise time, and when α approaches $\pi/2$, the time constant τ_r is equal to 96% of the rise time.) The time constant τ_{min} is the minimum rise time of the shaped pulse that can be obtained from the current pulse-shaping system. It is obvious from Eq. (11) that when the parameter α approaches $\pi/2$, the rise time τ_r approaches its minimum value τ_{min}. This time constant τ_{min} is also the shortest half pulse width (at e^{-1} amplitude point) of a Gaussian pulse that can be obtained by using a Gaussian spectral mask.[1] From Eq. (10) we know that the minimum rise time τ_{min} is proportional to the square root of the group delay per spectral width. Therefore, for a given group delay, the minimum rise time τ_{min} of the shaped pulse is determined by the input laser bandwidth $\Delta\omega$.

Figure 53.32 shows the unit-step-response curves of the laser intensity $|E_{out}(t)|^2$ with different values of tan α. When the spectral resolution N is large, the phase α approaches $\pi/2$ ($\tan\alpha \to \infty$) and the complex error function in Eq. (8) can be expressed by Fresnel integrals.[15] The temporal rippling of the shaped pulse in this case behaves exactly like Fresnel diffraction by a semi-infinite opaque screen. When the spectral resolution N is small, the phase α approaches zero, and the rippling disappears at the price of slower rise time. From Eqs. (9) and (11) we know that to reduce the temporal rippling (reduce α) we need to make a compromise with the rise time τ_r. When we choose $\alpha = \pi/4$ for Eq. (8), we find that the temporal rippling can be greatly reduced while the rise time τ_r does not increase significantly. This intensity response is shown by the thick solid curve in Fig. 53.32. We therefore apply tan $\alpha = 1$ to Eq. (9) and choose the optimal spectral resolution $N_{optimum}$ for the unit-step filtering system as

$$N_{optimum} = \frac{1}{2}\sqrt{\Delta\omega\Delta\tau}\ . \tag{12}$$

The easiest way to control the spectral resolution $N \equiv \Delta x/w_0$ is to adjust the size of the Gaussian beam waist w_0 on the spectral mask. Through the proper choice of the beam size on the spectral mask one can avoid the temporal rippling on the

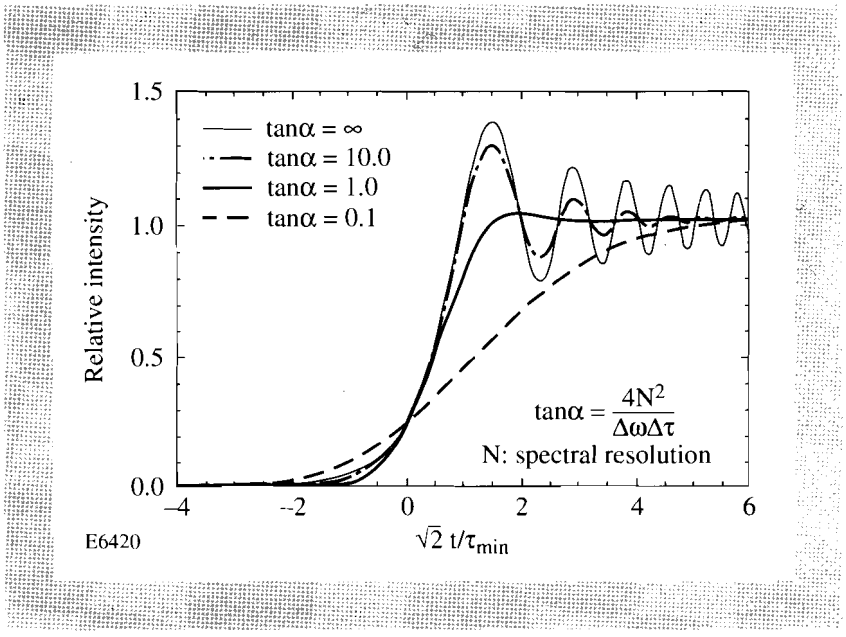

Fig. 53.32
The temporal-response curves of linearly chirped pulses shaped by a unit-step spectral mask. Limiting spectral resolution (thick solid line, tan $\alpha = 1$) can reduce the intensity rippling but still retain a good rise time.

shaped pulse without significant degradation of the rise time. Figure 53.32 also shows an important feature that at $t = 0$ the laser intensity rises to one quarter of its steady-state value and is independent of the parameter α. This was to be expected since half of the wavefront is obstructed by the spectral mask, the amplitude is halved, and the intensity drops to one quarter.

To obtain square pulses, one can immediately extend the previous unit-step spectral-filtering results to a square spectral window

$$M(x) = \begin{cases} 1 & x_1 \le x \le x_2 \\ 0 & \text{else} \end{cases} . \tag{13}$$

By applying Eq. (8) at $x = x_1$ and subtracting the unit-step response at $x = x_2$, the normalized laser intensity becomes

$$\left| E_{\text{out}}(t) \right|^2 = \frac{1}{4} \left| erf\left[e^{-i\frac{\alpha}{2}} \sqrt{2} \left(t - \frac{\Delta\tau}{\Delta x} x_1 \right) / \tau_r \right] - erf\left[e^{-i\frac{\alpha}{2}} \sqrt{2} \left(t - \frac{\Delta\tau}{\Delta x} x_2 \right) / \tau_r \right] \right|^2 . \tag{14}$$

Equation (14) shows that the time scales for both leading and trailing edges of the shaped pulse are equal to τ_r. As previously stated, one can adjust the spectral resolution N and the input laser bandwidth $\Delta\omega$ to obtain a square pulse with the desired rise time τ_r but without temporal rippling.

Schemes for Narrow-Bandwidth Pulses

Simple imaging systems can effectively provide the required grating separation for narrow-band pulses and at the same time control the laser-beam diffraction. Figure 53.33 schematically shows our first pulse-stretching-and-shaping system for narrow-band pulses, which consists of a pair of transmission gratings, a lens system including one down-collimator and one up-collimator, a spectral mask, and a retro-reflecting mirror. Four lenses with focal lengths f_1, f_2, f_3, and f_4 form the down-collimator and the up-collimator. Distances ℓ_1 to ℓ_6 describe the relative location of the optical elements. The spectral angular dispersion of the laser beam Γ ($\equiv d\theta/d\lambda$) is generated after passing through the first grating. The down-collimator magnifies the spectral angular dispersion from Γ to $M\Gamma$, where the magnification M is defined as

$$M \equiv -\frac{f_1}{f_2} = -\frac{f_4}{f_3} . \tag{15}$$

The up-collimator magnifies the spatial separation of different optical frequencies and returns the spectral angular dispersion from $M\Gamma$ back to Γ. The spectral angular dispersion is then cancelled by the second grating, which has the same groove spacing as the first grating but an opposite incidence angle. Two representative frequency components, denoted as λ_1 and λ_2, show the spectral

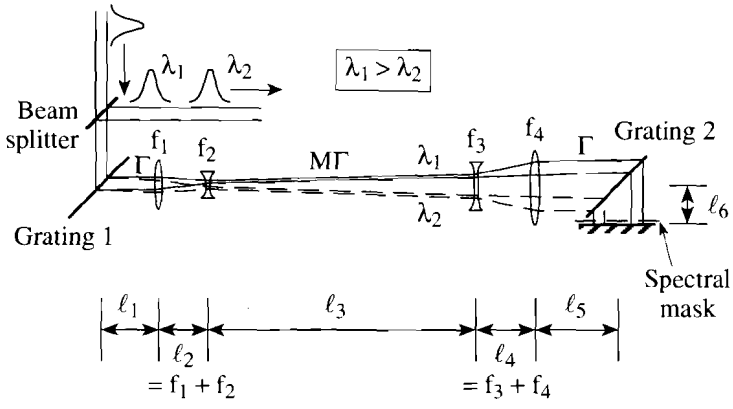

Effective grating separation: $L = M^2\ell_3 + M(f_1 + f_2 + f_3 + f_4) + \ell_1 + \ell_5$

E6421

Fig. 53.33

One down-collimator and one up-collimator effectively provide the required large effective grating separation. The down-collimator magnifies the spectral angular dispersion from Γ to $M\Gamma$. The up-collimator magnifies the spatial separation of different optical frequencies and returns the spectral angular dispersion from $M\Gamma$ back to Γ. The effective grating separation is $L = M^2\ell_3 + M(f_1 + f_2 + f_3 + f_4) + \ell_1 + \ell_5$, with $M \equiv -f_1/f_2 = -f_4/f_3$.

angular dispersion and the beam-size variation. Since the distance traveled by the λ_1 component is longer than the distance traveled by the λ_2 component, the output pulse will have a linear chirp.

The imaging system between the two gratings can be described by the well-known technique of ABCD matrices.[16] The ABCD matrices are developed from geometrical optics where an optical ray traveling a distance L is described by

$$\begin{bmatrix} x_2 \\ x_2' \end{bmatrix} = \begin{bmatrix} 1 & L \\ 0 & 1 \end{bmatrix} \begin{bmatrix} x_1 \\ x_1' \end{bmatrix},$$

and passing though a thin lens of focal length f is described by

$$\begin{bmatrix} x_2 \\ x_2' \end{bmatrix} = \begin{bmatrix} 1 & 0 \\ -1/f & 1 \end{bmatrix} \begin{bmatrix} x_1 \\ x_1' \end{bmatrix}.$$

The variables x_1 and x_2 are the input and output transverse displacements from the optical axis, and x_1' and x_2' are the slopes. In this manner we can obtain the spectral angular dispersion and the beam variation at the same time and can further apply the Huygen's integral to obtain the physical-optics results.[17] The ABCD matrix for the first optical system is obtained by writing the matrix for each component and distance and then multiplying. The result is

$$\begin{bmatrix} A & B \\ C & D \end{bmatrix}_I = \begin{bmatrix} 1 & L \\ 0 & 1 \end{bmatrix}, \tag{16}$$

where

$$L = M^2 \ell_3 + M(f_1 + f_2 + f_3 + f_4) + \ell_1 + \ell_5 \tag{17}$$

is the effective grating separation. Parameters ℓ_1, ℓ_3, and ℓ_5 represent the distances from the first grating to the down-collimator, from the down-collimator to the up-collimator, and from the up-collimator to the second grating, respectively. From Eq. (17) we know that the effective grating separation will be large if the magnification M is large.

Our second pulse-stretching-and-shaping system, shown schematically in Fig. 53.34, consists of the same optical components as the first system but with a somewhat more complicated arrangement, where $\ell_1 = f_1$, $\ell_2 = f_1 + f_2 + \Delta$, $\ell_4 = f_3 + f_4$. The laser beam leaving the first grating carries a spectral angular dispersion Γ. The first lens, which is placed at a distance $\ell_1 = f_1$ away from the first grating, cancels the spectral angular dispersion of the laser beam and makes all frequency components parallel to each other. Once these parallel frequency components pass the second lens (f_2) the spectral angular dispersion of the laser beam becomes $M\Gamma$ and is independent of the second lens position. We place the second lens at a distance $\ell_2 = f_1 + f_2 + \Delta$ away from the first lens. The small lens displacement Δ is used to control the beam diffraction and put the Gaussian beam

waist on the spectral mask $M(x)$. With this design the Fourier plane, which is formed by the beam waists of all frequency components, can be moved independently without affecting the spectral angular dispersion. The laser beam, after propagating a distance ℓ_3 away from the second lens, enters into a telescope formed by two lenses with focal lengths f_3 and f_4. This telescope, similar to the up-collimator in the first system, magnifies the spatial separation of different frequency components and returns the spectral angular dispersion from $M\Gamma$ back to Γ. The spectral angular dispersion is then cancelled by the second grating. The improvement of the spectral resolution caused by the displacement of the second lens can be understood by comparing the representative spectral components λ_1 and λ_2 in Figs. 53.33 and 53.34. Figure 53.34 shows a smaller Gaussian waist on the spectral mask for each frequency component.

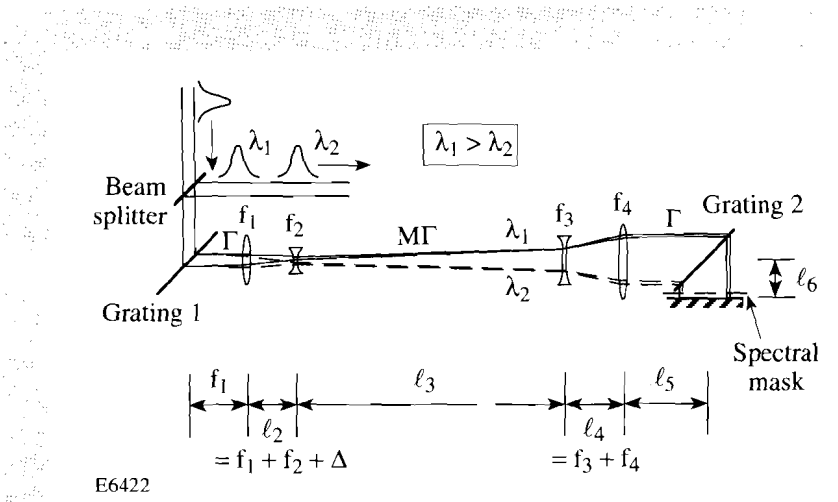

Fig. 53.34
The second spectral pulse-shaping scheme for narrow-band pulses: $\ell_1 = f_1$ and $\ell_2 = f_1 + f_2 + \Delta$. The second lens ($f_2$) is moved back a distance Δ to put the beam waist on the spectral mask. The spectral angular dispersion of the laser beam leaving the second lens is magnified to $M\Gamma$ and is independent of the second lens position.

The ABCD matrix for the second optical system is

$$\begin{bmatrix} A & B \\ C & D \end{bmatrix}_{II} = \begin{bmatrix} 1 - \dfrac{\Delta}{f_1^2} L & L \\ -\dfrac{\Delta}{f_1^2} & 1 \end{bmatrix} \tag{18}$$

The effective grating separation becomes

$$L = M^2 \ell_3 + M(f_1 + f_3 + f_4) + \ell_5 \,. \tag{19}$$

From $\ell_1 = f_1 = -Mf_2$ we know that Eqs. (17) and (19) are similar. The second optical system can also provide large effective grating separation if the magnitude of the parameter M is large. The ABCD matrix in Eq. (18) can be decomposed as

$$\begin{bmatrix} 1-\dfrac{\Delta}{f_1^2}L & L \\ -\dfrac{\Delta}{f_1^2} & 1 \end{bmatrix} = \begin{bmatrix} 1 & L \\ 0 & 1 \end{bmatrix} \begin{bmatrix} 1 & 0 \\ -\dfrac{\Delta}{f_1^2} & 1 \end{bmatrix}.$$

This is equivalent to a laser beam passing a lens with a focal length f_1^2/Δ and propagating a distance L.

We now apply the Gaussian beam analysis to our spectral pulse-shaping system as if the gratings were really separated a distance L.[17] For a collimated input beam, the second system can achieve significantly greater spectral resolution than the first. The axial position of the Gaussian beam waist of each frequency component in the second system is determined by the parameter Δ. To set the Gaussian waist on the spectral mask for a collimated input laser beam, the parameter Δ should be

$$\Delta = \frac{z f_1^2}{z^2 + z_R^2}, \tag{20}$$

where $z = L + \ell_6$ is the effective grating separation plus the distance from the second grating to the spectral mask, and $z_R \equiv k_0 w_0^2/2$ is the Rayleigh range of the Gaussian beam near the spectral mask. Equation (20) is obtained by matching the wavefront radius of curvature $z + z_R^2/z$ (see Ref. 16) to the overall focal length of the system f_1^2/Δ [Eq. (18)]. The relation between the input-beam size w_1 and the spot size on the spectral mask w_0 can be obtained from a Gaussian beam analysis

$$w_1 = w_0 \sqrt{1 + \frac{z^2}{z_R^2}}. \tag{21}$$

The spectral resolution of the system is limited by the laser-beam diffraction. For an input Gaussian beam with a beam waist w_1 at the first grating (collimated beam), the far-field diffraction half-angle is $\theta_d \equiv \lambda/\pi w_1$.[16] When the laser beam passes through the first grating, a spectral dispersion angle $\theta_\lambda \equiv \Gamma\Delta\lambda$ is added to the laser beam. To obtain the best spectral resolution we relay the Gaussian beam waist to the spectral mask where the beam waist $w_0 \approx \lambda L/\pi w_1 = \theta_d L$ [the limiting case $z >> z_R$ for Eq. (21)]. In this case the spectral resolution $N = \Gamma\Delta\lambda L/w_0$ approaches its maximum

$$N_{\max} = \frac{\theta_\lambda}{\theta_d}. \tag{22}$$

To increase the spectral resolution, one needs to increase the spectral dispersion angle θ_λ or decrease the diffraction angle θ_d. Increasing the grating angular dispersion Γ and the laser bandwidth $\Delta\lambda$ increases θ_λ. Increase of the input-beam size w_1 reduces θ_d. The input beam size w_1 is limited by the diameter of the first grating.

The system shown in Fig. 53.34 employs a novel way to obtain large group delay and high spectral resolution for narrow-band pulses. Figure 53.35 shows a multi-grating, folded-beam scheme in which a large group delay can be obtained with commonly available grating sizes. Two gratings in 67.5° Littrow mode are used as an example. The optical path traveled by the λ_1 component (solid line) is longer than that of the λ_2 component (dotted line) by an amount $16 D_2 \sin\theta$, where D_2 is the clear aperture of the second grating. For gratings with clear aperture $D_2 = 20$ cm, the optical path difference between λ_1 and λ_2 is about 3 m, which is equivalent to a 10-ns group delay. This grating arrangement can be used to replace the second grating in Fig. 53.34 to produce four-fold increase in the group delay. The spectral resolution can also be increased by a factor of 4 by replacing the first grating in Fig. 53.34 with the same grating arrangement as shown in Fig. 53.35, but with an opposite incidence angle.

The pulse-shaping systems described previously can provide large group delay and high spectral resolution for narrow-band pulses, though the pulse-shaping ability of the system is still limited by the laser bandwidth. From the unit-

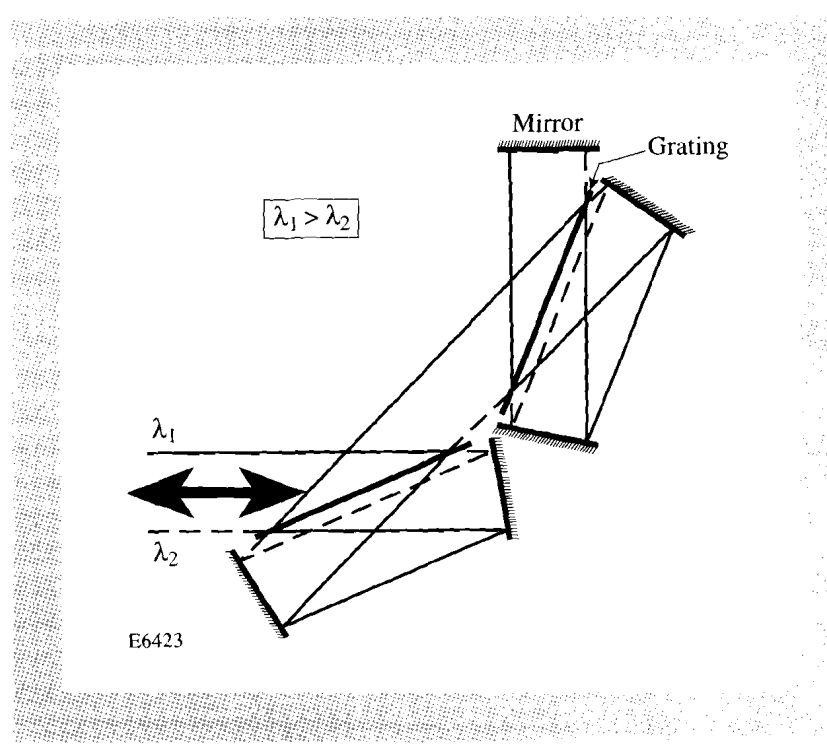

Fig. 53.35
A multi-grating, folded-beam scheme provides a large group delay with available grating sizes.

step-response analysis we know that the fidelity of the mapping from the spectral mask to the temporal pulse shape is determined by the minimum response time $\tau_{min} = 2(\Delta\tau/\Delta\omega)^{1/2}$. High spectral resolution allows the rise time τ_r to approach the minimum response time τ_{min}. However, the laser bandwidth $\Delta\omega$ must be large enough, for a given group delay $\Delta\tau$, to decrease τ_{min} to the desired amount.

Experiment

The purpose of this experiment was first to show the rise time and the flexibility of the spectral pulse-shaping technique and, secondly, to demonstrate the feasibility of the scheme for narrow-bandwidth pulses. The experimental setup follows the two-grating pulse-shaping scheme shown in Fig. 53.31. For shaping narrow-band pulses, the lens system shown in Fig. 53.34 was used to provide a large effective grating separation.

Figure 53.36 shows the details of the experimental setup for narrow-band pulses. A cw-pumped, mode-locked, Nd:YLF oscillator generates a 76-MHz train of ~77-ps pulses at a wavelength of 1053 nm. These pulses are coupled into a 2-km, single-mode optical fiber to generate the required bandwidth. Because of self-phase modulation and group-velocity dispersion occurring in the fiber, these pulses leaving the fiber can have a pulse width up to 240 ps and a bandwidth up to 30 Å. This bandwidth is wide enough for us to accurately study the minimum rise time of the shaped pulse versus the input laser bandwidth as described in Eq. (10). A 50% beam splitter transmits the input laser pulses and picks up the shaped pulses, which are sent back from the two-grating pulse-shaping system. The input laser beam, before entering the two-grating system, is collimated to different input beam sizes for different experimental conditions. The returned 2-mm laser beam, picked off by the beam splitter, is focused by a 200-mm focal-length lens into a 200-μm pinhole before entering into the streak camera. The spatial filtering reduces the effects of optical aberrations and ghost reflections that cause temporal modulation because of the interference effects from the space-to-time mapping. The time resolution of the streak camera used to measure the shaped pulse is ~14 ps.

The two-grating system shown in Fig. 53.36 is specifically for narrow-bandwidth pulses. Behind each grating two mirrors are used to double the angular dispersion and the group delay. The equivalent grating position of this folded-beam design is located midway between the two mirrors. Two transmission gratings are operated at 67.5° Littrow configuration. Both gratings have a 6-in. clear aperture and were holographically made using a new interferometric scheme.[18,19] The focal lengths of the lenses are $f_1 = f_4 = 600$ mm and $f_2 = f_3 = 80$ mm. For our convenience we have used positive focal lengths f_2 and f_3. Two turning mirrors are mounted on an optical rail and are used to adjust the optical path length between the f_2 lens and the f_3 lens (i.e., ℓ_3). The effective grating separation L described by Eq. (19) can be easily varied by shifting these two turning mirrors.

When aligning the f_1 lens, a retro-reflecting mirror is temporarily placed at the back focus of the f_1 lens. This mirror reflects the laser beam back to the beam splitter and the streak camera. The distance between the first grating and the f_1

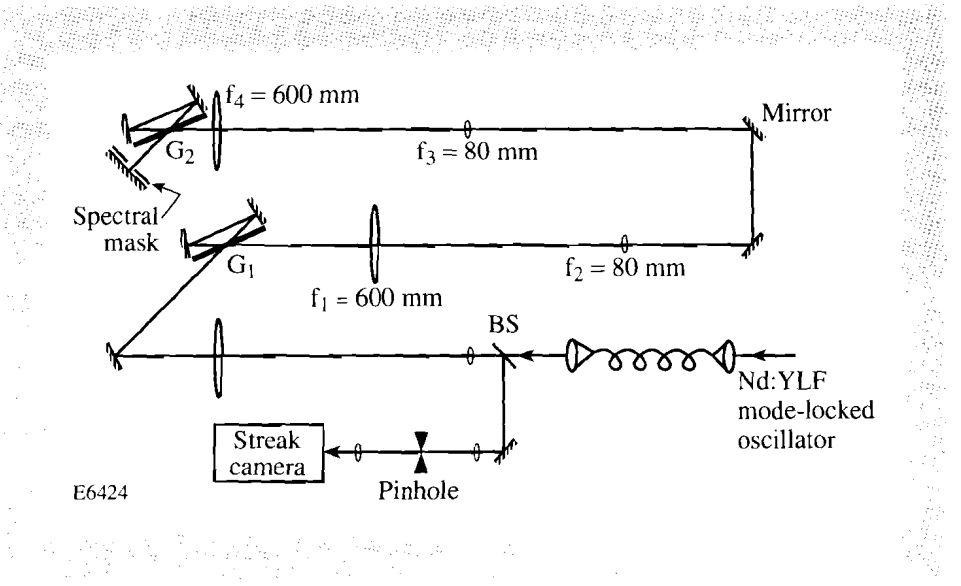

Fig. 53.36
Experimental setup for narrow-band pulses. BS: beam splitter; G_1 and G_2: transmission gratings.

lens is determined when no transverse-frequency chirp can be seen using the streak camera. The distance between the f_3 lens and the f_4 lens is accurately set using shearing interferometry. The second grating angle is carefully adjusted such that no transverse-frequency chirp can be seen using the streak camera. The fine adjustment of the f_2 lens position moves the Fourier plane to the spectral mask. We use an adjustable aperture (iris) in front of the system's retro-reflecting mirror as a binary spectral window to obtain square pulses. When shaping broad-bandwidth pulses, both the lenses inside the grating pair and the mirrors behind the gratings are removed, since the required grating separation is just several meters. The two-grating system is then like the one shown in Fig. 53.31.

Simple experiments and calculations demonstrate the performance of the spectral pulse-shaping system. Table 53.I shows the measured and calculated rise times of the stretched and shaped pulses under different frequency-chirp conditions: $\Delta\lambda/\Delta\tau = 20$ Å/ns, 5 Å/ns, 1 Å/ns, 0.61 Å/ns, and 0.13 Å/ns. In order to obtain this wide range of frequency chirp it is necessary to modify the two-grating setup in Fig. 53.36 to provide the required grating separation. For $\Delta\lambda/\Delta\tau = 20$ Å/ns, the lenses between the gratings and the mirrors behind each grating in Fig. 53.36 are removed. For $\Delta\lambda/\Delta\tau = 5.0$ Å/ns, the two mirrors behind each grating are installed to double the angular dispersion and shorten the required grating separation. For $\Delta\lambda/\Delta\tau = 1.0$ Å/ns and 0.61 Å/ns, the lens system is placed inside the grating pair as shown in Fig. 53.36, but the two mirrors behind each grating are removed. For $\Delta\lambda/\Delta\tau = 0.13$ Å/ns, the experimental setup is the same as in Fig. 53.36. The effective grating separations for the narrow-band cases, $\Delta\lambda/\Delta\tau = 1.0$ Å/ns, 0.61 Å/ns, and 0.13 Å/ns, are calculated from Eq. (19). The width of the spectral window $x_2 - x_1$ is adjusted so that a shaped pulse width of 1-ns (FWHM) is obtained. In each case, the spectral resolution is adjusted to

the optimal value [Eq. (12)] by controlling the beam waist w_0. The minimum rise time τ_{min} and the rise time τ_r at $\alpha = \pi/4$ are calculated from Eqs. (10) and (11), respectively. Table 53.I shows that the measured rise times are well located between the calculated minimum rise times τ_{min} and the estimated rise times τ_r.

Table 53.I: Measured and calculated rise times in different experimental conditions.

$\Delta\lambda/\Delta\tau$ (Å/ns)	Measured rise time (ps)	τ_{min} (ps)	τ_r ($\alpha = \pi/4$) (ps)	Two-grating system	L (m)	$x_2 - x_1$ (mm)	w_0 (mm)
20	34±7	34	40	No imaging No folding	4.2	38	2
5.0	78±7	68	81	No imaging Folded beam	4.36	17	1.5
1.0	175±11	153	182	With imaging No folding	67.5	35	5
0.61	201±11	198	236	With imaging No folding	111	35	6
0.13	501±30	424	505	With imaging Folded beam	132	20	7

E6533

Figure 53.37 shows experimental (solid lines) and calculated (dotted lines) pulse shapes of the stretched and shaped pulses for cases (a) 20 Å/ns, (b) 5 Å/ns, (c) 1 Å/ns, and (d) 0.13 Å/ns. The theoretical curves are obtained from numerically solving Eqs. (1) and (2) and are further checked against Eq. (8). The parameters $L, x_2 - x_1$, and w_0, used in this calculation, are listed in Table 53.I. In all cases, the rising (or trailing) edges of both theoretical curves and experimental results are very well matched.

The intensity (energy) noise near the peak of each experimental curve does not randomly vary during the course of many measurements. It was found to be fixed and different for each experimental setup. The noise is produced from several sources. The defects on the second grating affect the diffraction efficiency for each frequency component of the laser beam and imprint the noise on the output-shaped pulse. This noise can be identified by moving the grating such that the noise pattern changes as the grating moves. Also, etalon effects produced from transmission gratings and other optics cause beat patterns on top of the linearly chirped pulse.[4] Wedged optics should be used in shaping of linearly chirped pulses. In addition, lens aberrations can change the characteristics of the laser-beam waist on the Fourier plane and affect the shaped pulse. This noise can be reduced by spatially filtering the shaped laser beam. Each of these sources of noise can be eliminated with higher quality optical elements.

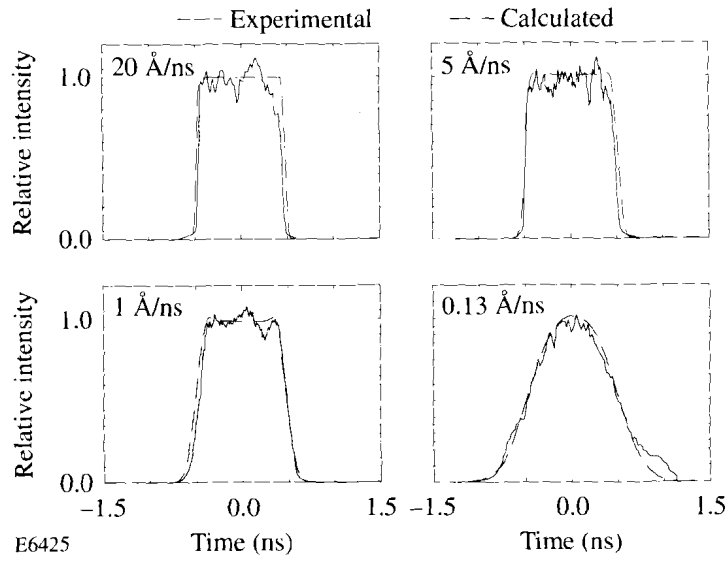

Fig. 53.37
Experimental (solid lines) and calculated (dotted lines) results of the stretched and shaped pulses under different frequency-chirp conditions: (a) 20 Å/ns, (b) 5 Å/ns, (c) 1 Å/ns, and (d) 0.13 Å/ns. The measured rise times are (a) 34 ps, (b) 78 ps, (c) 175 ps, and (d) 501 ps.

To show the flexibility of the spectral pulse-shaping technique we present the two shaped pulses shown in Fig. 53.38. The experimental setup is that shown in Fig. 53.36 without modification. The experimental parameters are $L = 27$ m and $w_0 = 1$ mm. The frequency chirp is 0.6 Å/ns. These two pulses are arbitrarily shaped using a simple binary mask in the spectral plane. The flexibility of this technique is currently limited by the availability of masks with variable-gray levels. However, from this simple demonstration we can infer that the spectral pulse-shaping technique is capable of producing a wide range of pulse shapes. System flexibility is important for later studies, using the OMEGA Upgrade, of how target performance is affected by laser pulse shapes.

Conclusion

This article has reported on all optical techniques for shaping and stretching nanosecond linearly chirped pulses. The fidelity of the mapping from the spectral mask to the temporal pulse shape for a linearly chirped pulse has been shown to be dependent on the laser bandwidth, the frequency chirp, and the spectral resolution. Proper design of these parameters leads to fast rise times and stable, smooth pulse shapes. A pulse-stretching scheme for narrow-band pulses was also presented and tested in this study. This spectral pulse-shaping technique provides the required stability, flexibility, and fast rise times necessary for laser-fusion research. Future investigation will include the injection of shaped pulses

into a regenerative amplifier, the generation of linearly chirped pulses from electro-optical modulators, the use of a zero-dispersion pulse-shaping scheme, and the deployment of a liquid-crystal, spectral-light modulator for flexible mask generation.

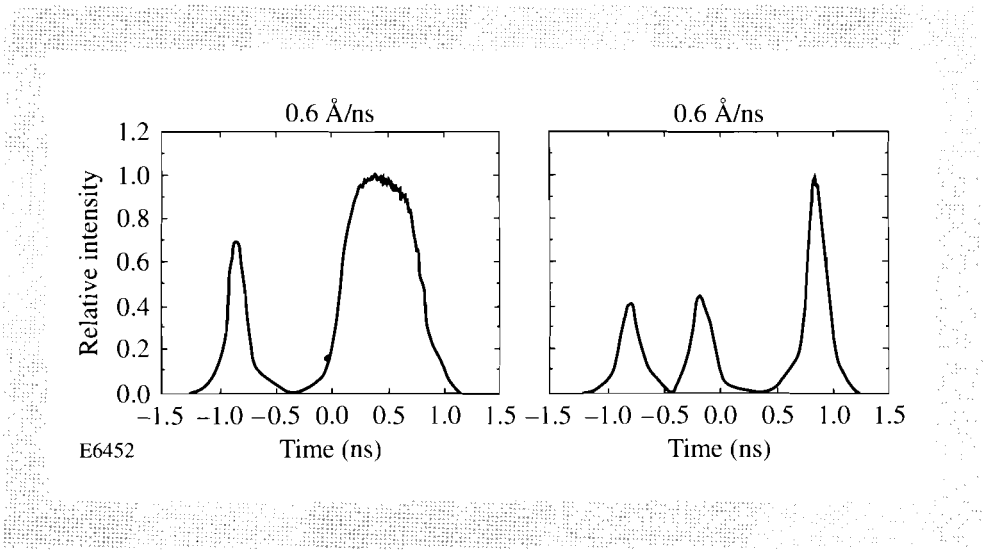

Fig. 53.38
Simple examples of shaped pulses showing the spectral pulse-shaping technique capable of producing a wide range of pulse shapes. The frequency chirp is 0.6 Å/ns for both cases.

ACKNOWLEDGMENT

The authors would like to thank J. Armstrong for providing the transmission gratings and C. Kellogg for his assistance. This work was supported by the U.S. Department of Energy Office of Inertial Confinement Fusion under Cooperative Agreement No. DE-FC03-92SF19460, the University of Rochester, and the New York State Energy Research and Development Authority. The support of DOE does not constitute an endorsement by DOE of the views expressed in this article.

REFERENCES

1. S. Skupsky, T. Kessler, S. Letzring, and Y.-H. Chuang, submitted to the Journal of Applied Physics.
2. E. B. Treacy, IEEE J. Quantum Electron. **5**, 454 (1969).
3. J. Desbois, F. Gires, and P. Tournois, IEEE J. Quantum Electron. **9**, 213 (1973).
4. J. Agostinelli *et al.*, Appl. Opt. **18**, 2500 (1979).
5. J. P. Heritage, A. M. Weiner, and R. N. Thurston, Opt. Lett. **10**, 609 (1985).
6. A. M. Weiner, J. P. Heritage, and R. N. Thurston, Opt. Lett. **11**, 153 (1986).
7. R. N. Thurston *et al.*, IEEE J. Quantum Electron. **22**, 682 (1986).
8. O. E. Martinez, J. P. Gordon, and R. L. Fork, J. Opt. Soc. Am. A **1**, 1003 (1984).
9. O. E. Martinez, IEEE J. Quantum Electron. **23**, 59 (1987).

10. O. E. Martinez, IEEE J. Quantum Electron. **24**, 2530 (1988).

11. A. M. Weiner *et al.*, IEEE J. Quantum Electron. **28**, 908 (1992).

12. LLE Review **39**, 114 (1989).

13. S. Skupsky, R. W. Short, T. Kessler, R. S. Craxton, S. Letzring, and J. M. Soures, J. Appl. Phys. **66**, 3456 (1989).

14. R. S. Craxton, IEEE J. Quantum Electron. **17**, 1771 (1981).

15. *Handbook of Mathematical Functions with Formulas, Graphs, and Mathematical Tables*, edited by M. Abramowitz and I. A. Stegun (Dover, NY, 1970), p. 301; $erf\left[\left(\sqrt{\pi}/2\right)(1-i)z\right] = (1-i)\left[C(z) + iS(z)\right]$, where $C(z)$ and $S(z)$ are Fresnel integrals.

16. A. E. Siegman, *Lasers* (University Science, Mill Valley, CA, 1986), Chaps. 15–17, 20, and 21.

17. Y.-H. Chuang, T. J. Kessler, S. Skupsky, and D. L. Brown, submitted to the IEEE Journal of Quantum Electronics.

18. J. J. Armstrong, Masters thesis, University of Rochester (1992).

19. LLE Review **50**, 61 (1992).